ATLAS muon chamber construction at NIKHEF

NIKHEF ATLAS MUON GROUP
Contact: Marcel Vreeswijk, h73@nikhef.nl

November 2005

Abstract

At NIKHEF (Amsterdam), the largest muon chambers for the outer layer of the barrel ATLAS muon spectrometer have been constructed. At this facility, more than 40000 single drift tubes have been produced and 100 drift tube assemblies (muon chambers) have been constructed. We report on the quality assurance of both single drift tube production and chamber assembly. This, together with the also presented results from X-ray scans at CERN (Geneva) and results obtained in a dedicated cosmic ray test set-up, also part of the facility, demonstrates that the chambers fulfil ATLAS specifications.

Contents

List of Figures

1 Introduction

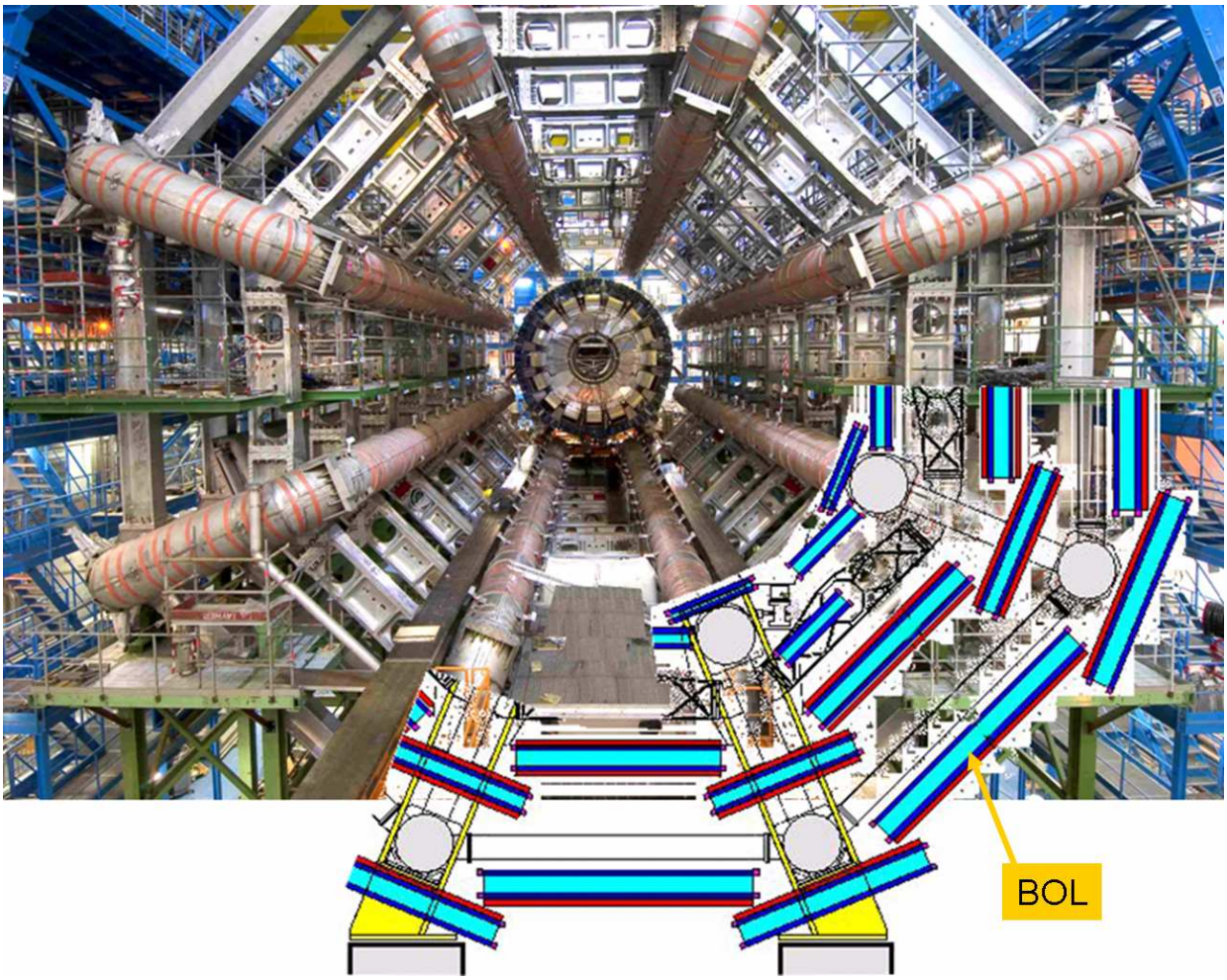

Figure 1: *Picture taken in the fall of 2005 of the ATLAS detector under construction. The muon system will be installed on the support structures of the eigth coils (the 'eight leg star' shape in the picture) that provide the toroidal magnetic field. On the bottom-right part of the picture, a drawing of a cross sectional view of the muon spectrometer is displayed, together with the feet that carry the ATLAS detector. This gives an impression of the location and size of the three layers of muon stations. The largest type of the outer layer, the BOL chamber is indicated. In the longitudinal direction (pointing in the paper) 12 muon chambers are positioned of each type. In the center of the picture, the calorimeter (not yet at its final position) is visible.*

To stand-alone measure muons that emerge with a transverse momentum of 1 TeV/c with an accuracy $\frac{\sigma_{P_T}}{P_T}$=10% is the most stringent requirement for the muon spectrometer of the ATLAS experiment at the LHC. This translates to 50 μm uncertainty on the sagitta measurement in the 2 Tm integrated magnetic field, provided by an air core toroid.

The muon system in the barrel region ($\eta < 1$) is designed such that muon trajectories are measured by three muon chambers as illustrated in figure 1. All three layers consists of an approximately equal number of small and large type chambers. At NIKHEF (Amsterdam, The Netherlands) we constructed 100 'Barrel Outer Large' (BOL) chambers, including four spare chambers.

Muons chambers consist of accurately assembled layers of alumnium drift tubes. A drift tube has a diame-

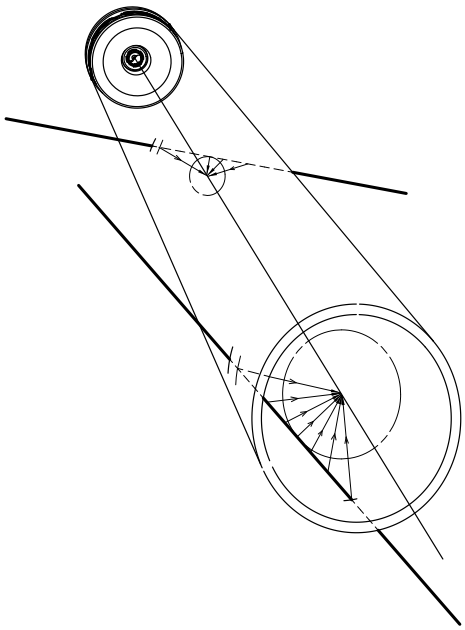

Figure 2: *Illustration of the MDT measurement principle. The figure shows two muons entering a drift tube. One of the muons (the one in the back) passes relatively close to the wire and thus has small drift distance as indicated by the circle with corresponding radius. The other muon passes wire at a large distance as indicated.*

ter close to 3 cm and is closed by two end-plugs that hold a 50 μm thick tungsten wire. Under operational conditions, the tube is filled with an Ar/CO_2 mixture of 93%/7% and the wire is set a potential of 3100 V (gas gain 2×10^4) with repect to the grounded tube wall. When a muon traverses the tube, it ionises the gas and the free electrons drift to the wire, generating a signal as illustrated in figure 2. The Read-Out electronics measure the arrival time of the signal above an adjustable threshold. The arrival time, containing the actual drift time information, is offline used to determine the drift radius based on a known relation between drift time and radius. Earlier tests (see [1]) show that the drift tubes under well-controlled conditions have single hit resolution of about 80 μm (averaged over drift distance). The muon chambers in ATLAS have each at least 2×3 drift tube layers, providing sufficient drift radii to recognize and reconstruct a track segment with high accuracy.

The BOL muon chambers consists of two separate layers (multi-layers), each with three drift tube layers, mounted on an aluminium support structure (spacer) as shown in figure 3. Physical deformations of the chambers during construction, transport and operation are monitored [1] with an integrated, so called 'in-plane', alignment system also indicated in figure 3.

The combination of the uncertainties on single hit resolution, alignment and mechanical precision of the chambers should not exceed 50 μm to meet the aforementioned accuracy on the sagitta measurement. Consequently, obtained from simulations, the mechanical precision of the chambers is required to be 20 μm (RMS), which is of unprecented accuracy for such large detectors.

[1] For this reason the ATLAS muon chambers are called Monitored Drift Tube (MDT) chambers

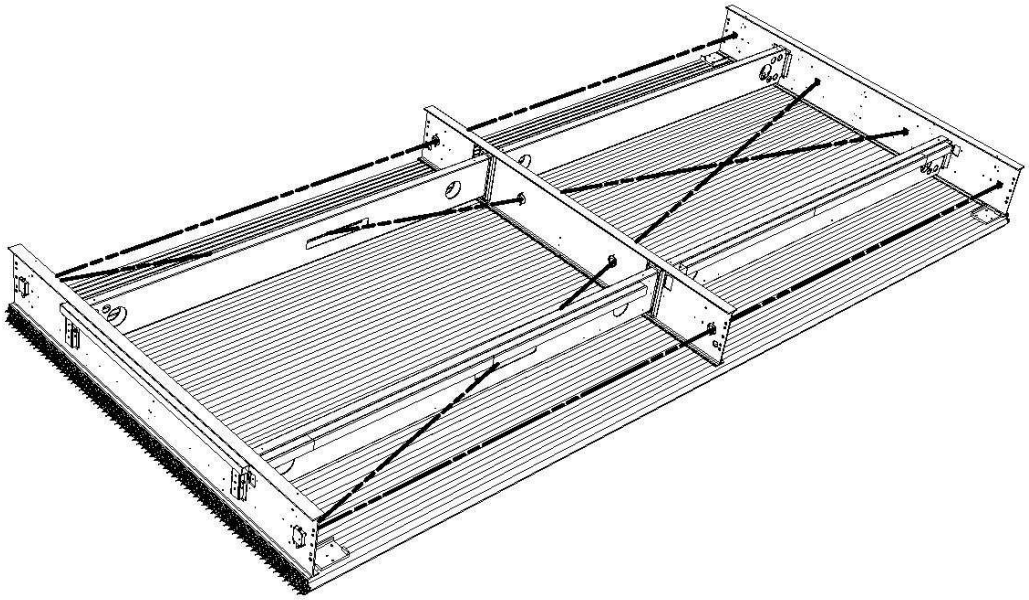

Figure 3: *Schematic view of a muon chamber without the upper multilayer. The drift tube layers are mounted on a support structure with integrated alignment system that consists of two parallel and two diagonal light rays indicated as black lines.*

In this report, we describe the production of single tubes and completed BOL chambers, moreover we present the results on the quality assurance operations. Among the tests is the dedicated measurement in the X-ray tomograph at CERN of a limited number (roughly 10%) of the BOL chambers. Finally, we summarise the muon chamber performance in the cosmic ray set-up at our facility.

2 Drift tubes

A schematic view of a drift tube is shown in figure 4. A drift tube has a diameter of 29.970 $\pm$ 0.015 mm

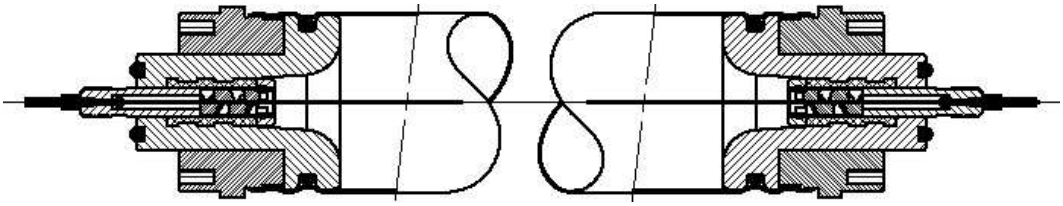

Figure 4: *Schematic view of the coss section of a drift tube with its end-plugs that hold the wire.*

and a wall thichness of 400 μm . The tube is swaged on two precise end-plugs that are manufactured with a precise outer ring of aluminium to position the tube during the assembly in jigs with high precision. The end-plug also connects to the gas system and is closed by a signal cap to connect High Voltage (HV) and Read-Out (RO) electronics boards at the tube's HV and RO ends respectively.

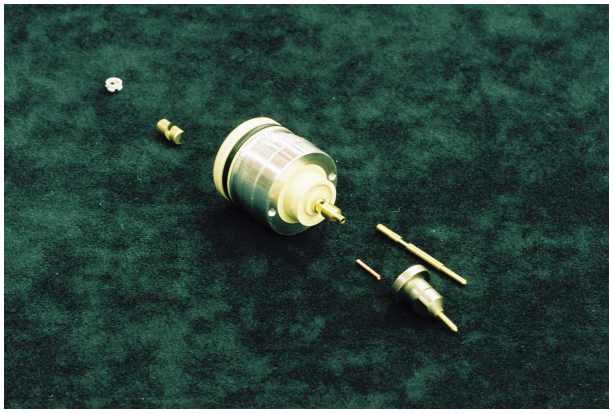

Figure 5: *Picture of an end-plug and its components. From left to right along the plug axis: plastic cap to fix the twister, the twister, the end-plug main body with a O-ring, the crimping pin and signal cap. The long pin next to the signal cap connects to the ground on the electronic board.*

The 50 μm gold-plated tungsten wire is tensioned at 285 gram and then crimped into the end-plug. A locator ('twister') with small gas flow resistance, accurately centres the wire with respect to its outer ring.

2.1 Drift tube requirements

The contribution of individual drift tubes has to remain well below 20 μm to accomodate the finite accuray of the tube positioning during chamber assembly. This imposes several requirements on the design and production of the the drift tubes:

- The end-plugs and wire locators, which determine the position of the wire near the tube ends, need to be machined with high accuracy. We required the precision rings be machined within 10 μm with respect to the axis of the endplugs.
- Near the middle of the tube, away from the endplugs, the wire tension determines the position of the wire (with respect to the precision ring). The wires of the BOL chambers are tensioned at 285 gram, which corresponds to a maximal gravitational sag of 406 μm . To limit the uncertainty (RMS) on this value to 10 μm precision an accuracy of 7 gram is required on the wire tension.
- The requirement on the co-centricity of the wire due to non-straightness of the drift tube (anode-cathode distance) is a second order effect and set at 100 μm RMS.

Other than mechanical precision we require:

- the dark current of individual drift tubes shall not exceed 10nA at 3400V at 3bar absolute pressure with an Ar/CO_2 (93%/7%) gas mixture,
- the leak rate under these conditions must be less than 10^{-8} bl/s.

These requirements ensure long term stable operation in the ATLAS experiment.

2.2 Drift tube production

The 40 thousand drift tubes are produced in the temperature-controlled cleanroom parallel to the assembly of the chambers, using a semi-automated wiring machine. On the picture shown in figure 6, taken at the south side (as we define it), several components are shown.

The machine is loaded by an aluminium tube and two complete endplugs. The wire is transported from its supply by means of airflow through the 'south' end-plug toward the 'north' end of the tube. At the north end the wire is literally sucked through the end-plug and fetched by a wire clamp. Now, movable platforms at both sides bring the end-plugs to their final positions in the tube. The two end-plugs are fixed by tube swager using air pressure. At the south end, the wire is fixed at the left end-plug by crimping it and the tube is in the state as shown in the picture. The clamp at the other side moves away to pre-tension the wire by 400 gram before releasing it slowly to its final tension of 285 gram. Crimping the wire at the north end-plug finalises the drift-tube.

2.3 Drift tube quality

The wire tension, length and position was measured immediately after production for every tenth tube to assure proper operation of the wiring machine.

The tension is derived from the measurement of the fundamental harmonic resonance. This measurement is als used in [2] and it is based on the induced response to a sinusoidal current while the tube is partially immersed in a magnetic field.

The wire position with respect to the outer ring of the end-plug was measured using an eletromagnetic method (see [3]). the method uses the response of two coils sensing the field of an sinusoidal current that is driven through the wire. One set of coils is used at each end of the tube and by rotating the tube by 90 degrees two projections (called y and z) for each end are obtained.

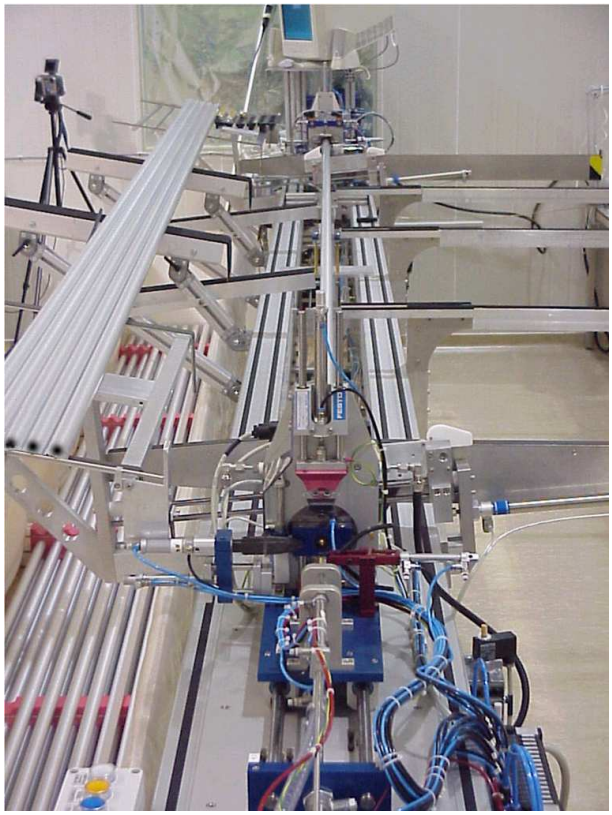

Figure 6: *Picture of the wire machine taken at the south side. On the left the empty tubes come in. The tube in the center is being wired and will roll off at the right, where futher quality checkes are performed.*

Figure 7a shows a scatter plot of these projections. The radial deviation is better than 10 μm (RMS) as appropriate. In these tests, we found only eleven tubes with a deviation larger than 25 μm in one of these projections, which we stored for further (destructive) studies.

The gas tightness and dark current of all produced tubes was measured in a set-up (in the cleanroom) specially designed for this purpose. This set-up consists of 80 vacumized large tubes (diameter 6xxxx cm) loaded with the drift tubes under test. The drifttubes are filled with 4 bar 1%/99% helium/argon mixture and the wire is set at 3400 V. The leakrate (for Ar/CO_2 at 3 bar) and dark current measurement is shown in figure 8 and 9 respectively. The results indicate that the majority of the tubes is well within specifications. However, the long tail of the leakrate distribution (not shown) leads to a failure rate of about 1%, making the leakrate the dominant rejection source.

After ageing of at least one month and just prior to using the tubes in the actual chamber assembly, all the tubes have been subjected to a second wire tension test. Like the frist measurement, the tension is also derived from the measured resonance frequency, but without the requirement that the tube is immersed in an magnetic field. The electrostatic force due to a supplied sinusoidal HV leads to mechanical wire oscillations. The changing capacity of the tube is measured in an LC circuit, leading to a resonance curve. the method is described in [4]. For our wire with length 4940 mm a weight per unit length of 38.70 mg/m, a resonance frequency of 27.2 Hz corresponds to 285 gram. The results of the second tension measurement are shown in figure 10. The precision of the wire tension over the full period of time is 0.33 Hz, which corresponds to about 6 gram (or 8 μm maximal sag). We decided to reject tubes with deviations larger than 1.5 Hz away from the nominal value, which led to the rejection of 21 tubes.

As mentioned above, for 10% of the tubes a 'fresh' measurement of the wire tension is available, allowing to study 'slippage' that may occur over time. We expect that if any slippage occurs, it occurs dominantly in the in the ageing period and possibly during handling of the tubes. The change in resonance frequency exhibits an assymetric shape as shown in figure 11. This suggest a comfortably small wire slippage for a

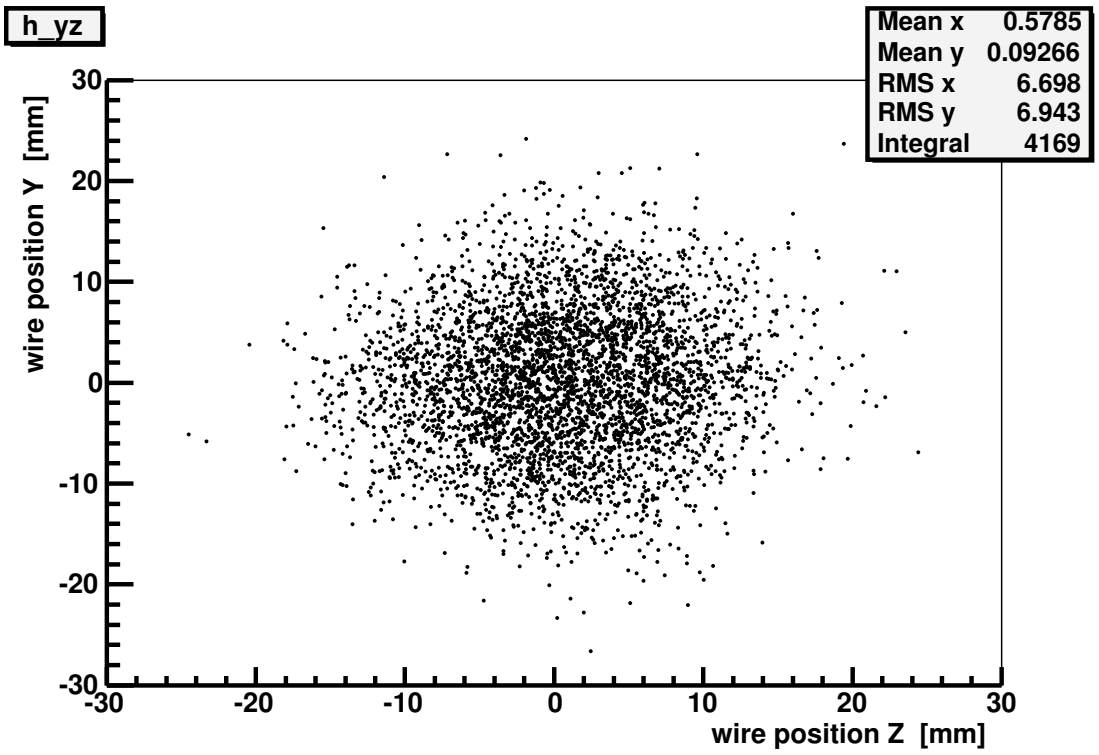

Figure 7: *Scatterplot of the y and z deviation of the wire position measured on a sub-sample of produced drift tubes.*

fraction of the tubes.

In total, we have produced about 40000 drift tubes. Our stringent criteria led to a rejection rate of 2.5%. The 100 BOL chambers (96 ATLAS chambers and 4 spares) we produced, contain only tubes that fullfil our requirements.

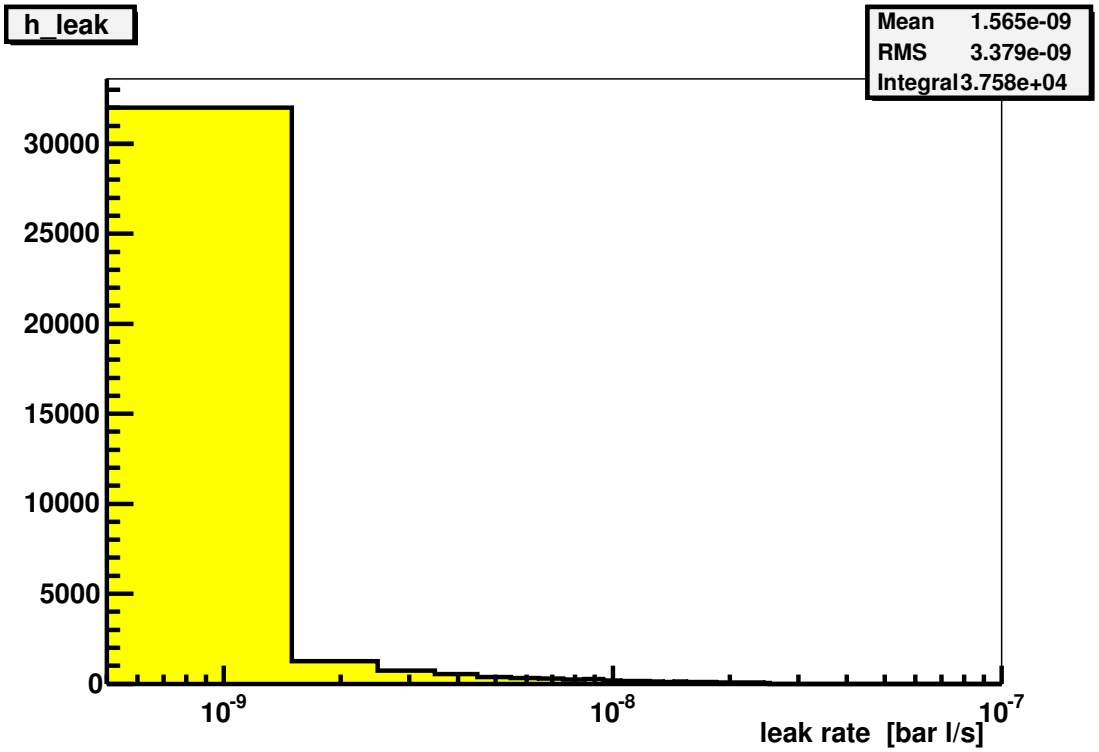

Figure 8: *Leakrate of all used tubes in b l/s*

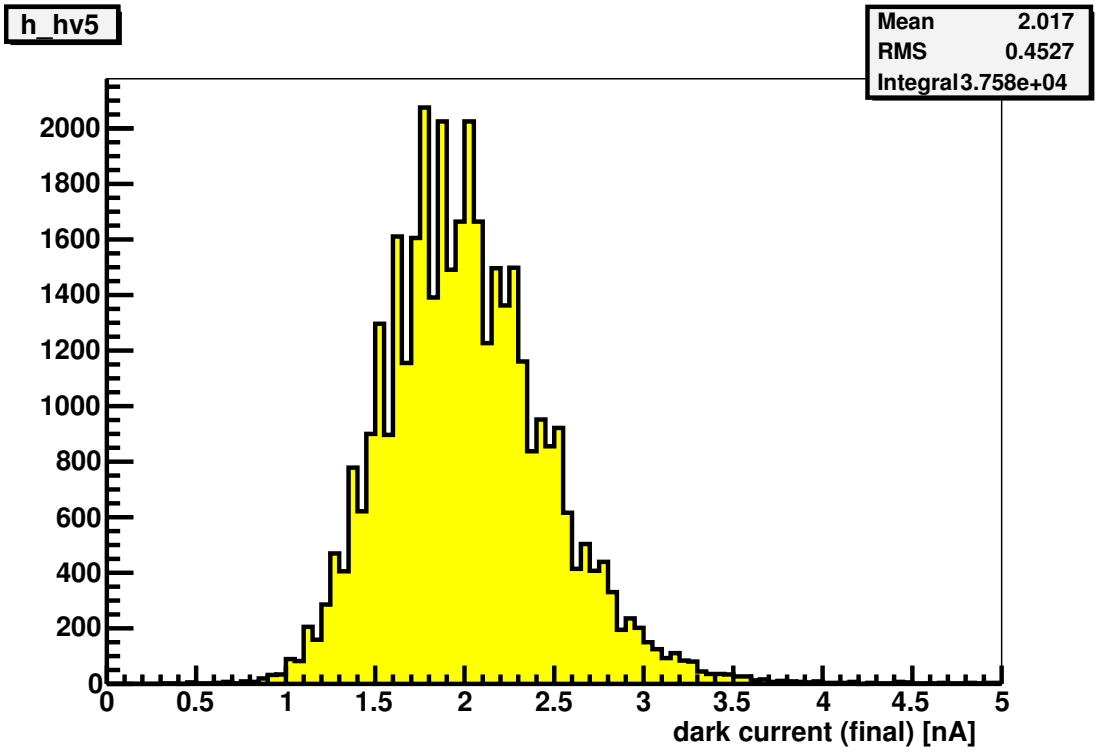

Figure 9: *a: Dark current in nA of all used tubes.*

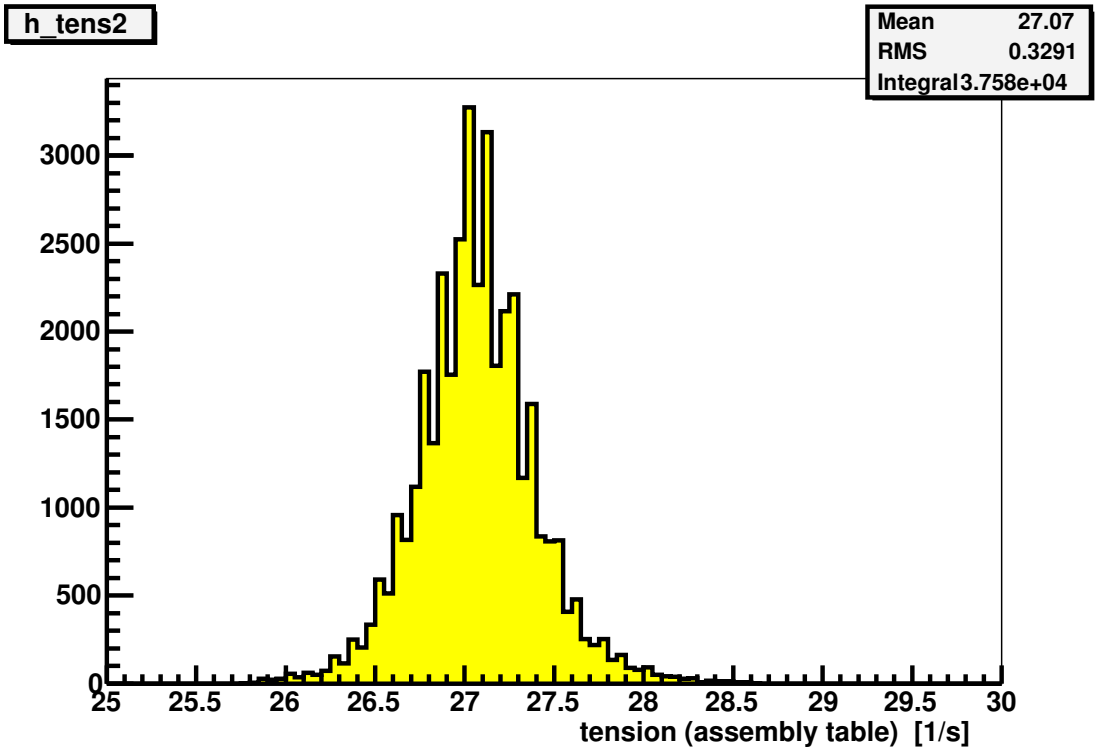

Figure 10: *Measurement of the wire tension of all tubes just before chamber assembly.*

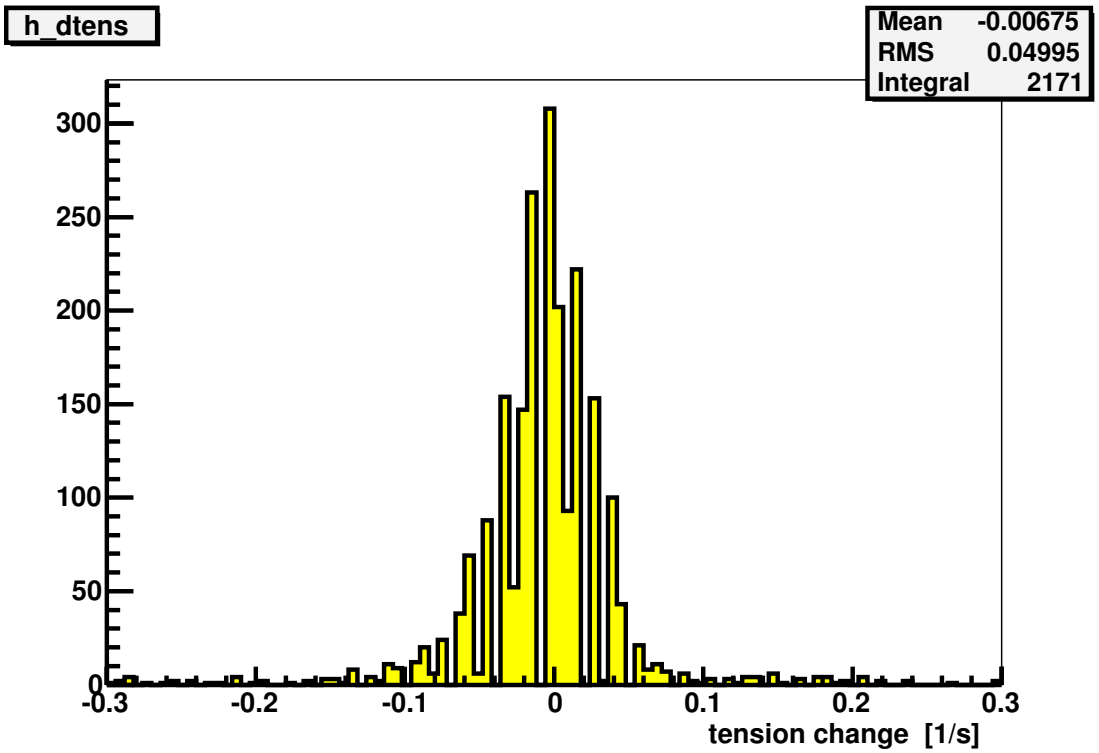

Figure 11: *Measurement of the change in wire tension between production of the tube and chamber assembly.*

3 Drift tube chambers

Above we already showed in figure 3 the mechanical layout of a BOL chamber. The aimed mechanical precision of 20 μm RMS is implemented as follows. Any transverse cross section of any chamber can be represented by a single wire grid. The individual wires of a particular chamber are mapped on this grid with residuals distributed within 20 μm RMS. Note that this precision applies to the wires, while the tubes have a looser position requirement of 100 μm RMS (with respect to the wire).

The BOL chambers have a length of 5 m and come in three different widths: 2160 mm (72 tubes/layer), 1680 mm (56 tubes/layer) and 1440 mm (48 tubes/layer), all with two multilayers with 3 tube layers on each side of the spacer.

The spacer is constructed of three 'I' beams, called cross-plates, running orthogonal to the tubes. The cross-plates have low mechanical precision (0.5 mm) and the glue, which connects to the mulilayers, absorbs possible irregularities. The crossplates are connected by two beams, that run longitudinal (which are therefore called long-beams). The horizontal position of the central cross-plate with respect to the long-beams is adjustable to compensate for gravitational sag of the chamber. A schematic view of the sag adjustment system is shown in figure 12.

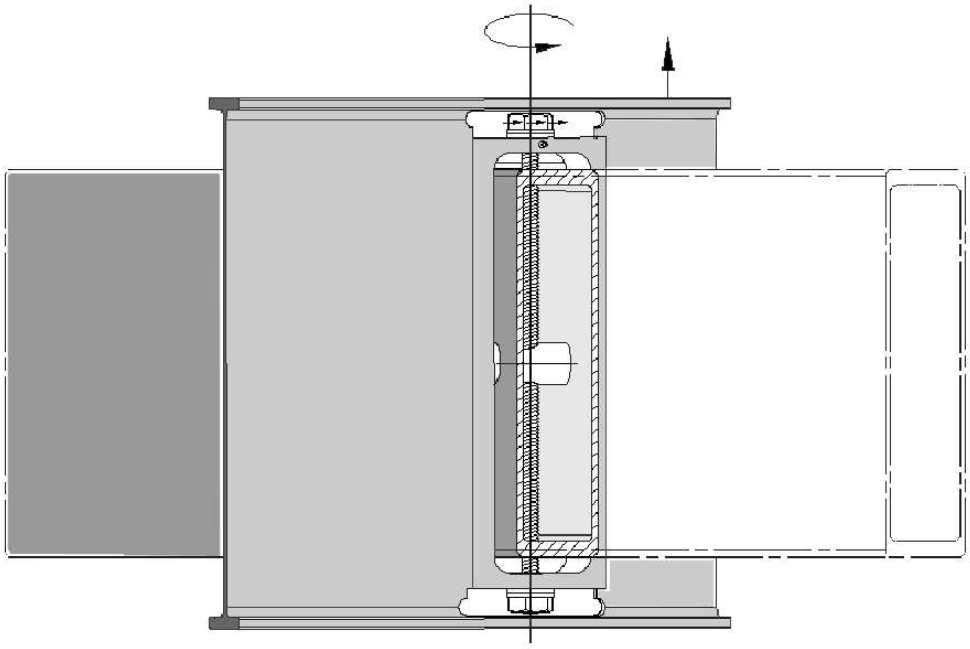

Figure 12: *Schematic view of the sagadjustment system in the central cross-plate. Shown is the longbeam that is connected to this cross-plate with a SPINDEL. By simply turning the SPINDEL the heigth of the central cross-plate with respect to the longbeam is adjusted, enabling to align the central crossplate with respect to the outer cross-plates.*

For the in-plane alignment system, two camera's and four masks are mounted on the, so called, RO and HV cross-plates of the chamber respectively and the central crossplate houses four lenses. With two parallel and two diagonal light rays several deformations of the spacer and thus chamber can be monitored; most notably the sag and torque of the chamber. The torque is a relative rotation of the two outer cross-plates. A total of 18 temperature sensors are mounted on the crossplates to monitor temperature gradients.

Tubes of the same layer lie in the same plane. The tubes of an adjacent layer is shifted by 15 mm (the half of the tube's width) and stacked as illustrated in figure 13.

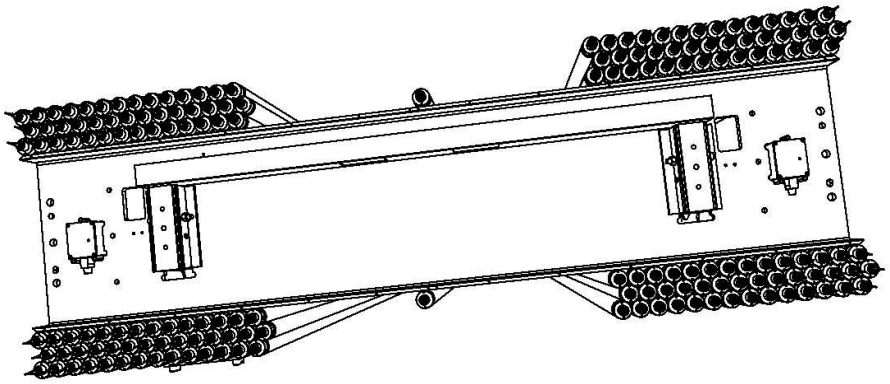

Figure 13: *Schematic view of a chamber with several tubes left out to illustrate the stacking of tubes into layers.*

Tubes of the same layer are grouped in series of three (tripplets) to reduce the number of gas connections to the on-chamber manifold. Only the first and last tube in the triplet connects to the manifold at the RO side and HV side respectively, while the tubes are connected with plasticxxxxx gas jumpers. The mounting of electronic boards, equipped with xxxxconnections, is carefully prepared by fixing the rotation of the tubes such that the ends of the ground pins finally line up within 0.5 mm. In the next chapter we elaborate on the on-chamber services.

Practically, the position requiment of 20 μm on the wires implies that the drift tubes should be accurately assembled into a chamber near the endplugs at the outer cross-plates. The straightness of the tubes in between the endplug is of less importance. Therefore, we aimed to set-up an assembly stand based on a granite table with precision mechanics, such as jigs to hold the drift tubes, machined with a precision of 10 μm or better. During assembly, the position of the spacer and individual tubes near the outer cross-plates need to be monitored to the same level.

3.1 Assembly station

The gluing of six layers of 72 tubes onto a structure with dimensions 5m $\times$ 2m , with a precision of 20 μm is a delicate procedure. Depending on the actual layer to be glued, mistakes are costly in time and material. We constructed an accurate assembly station and adopted a robust procedure to assemble the muon chambers with high precision. A picture of a mecanically completed BOL chamber on the assembly station is shown in figure 14. Below, we describe in detail the setup and the assembly steps.

Figure 14: *finished BOL*

Figure 15 shows the granite table equipped with precision mechanics. The cartesian coordinate system and the north (N), south (S) and west (W) sides are also indicated. When the chamber is located on the assembly station in the 'upward' position the local chamber coordinates are defined such that the y coordinate points to the sky, the x coordinate runs along the tubes in the horizontal plane. The z coordinate, the precision coordinate, runs perpendicular to the tubes. The x, y and z axis constitute a right-handed coordinate system. In the 'upward' position, the Read-out (RO) and High-Voltage (HV) side of the chamber coincides with the south and north respectively. In addition, for engineering purposes, we defined the west side of the setup as the 'reference-side'. The reference side always coincides with the smallest z coordinate of the chamber.

All jigs are equipped with vacuum suckers to hold the tubes firmly positioned. The end-plugs are hold by the outer jigs, which are constructed and positioned with a tolerance of 10 μm . The jigs are fixed at the west side, the reference side, and can expand freely to absorb temperature variations. These components, combined with a stable and uniform temperature (typical variation $< 0.5\,^{\circ}$C over one day) allow to assemble chambers within the 20 μm RMS precision requirement.

During assembly, extensions with precise spheres (diameter 6cmxxxx) are mounted on the cross-plates as can be seen in figure 16a. These extension house a RASNIK-mask, monitored by the so called RASNIK monitoring system as indicated in the figure. The principle of the RASNIK alignment is explaned in Appendix A. Using exchangable blocks (also indicated in the figure), the stacking towers have adaptable heights to absorb the thickness of the vertical (y) pitch of the tube layers. The central stacking position is shifted by half the horizontal (z) pitch as appropriate. The stacking towers at the reference side support

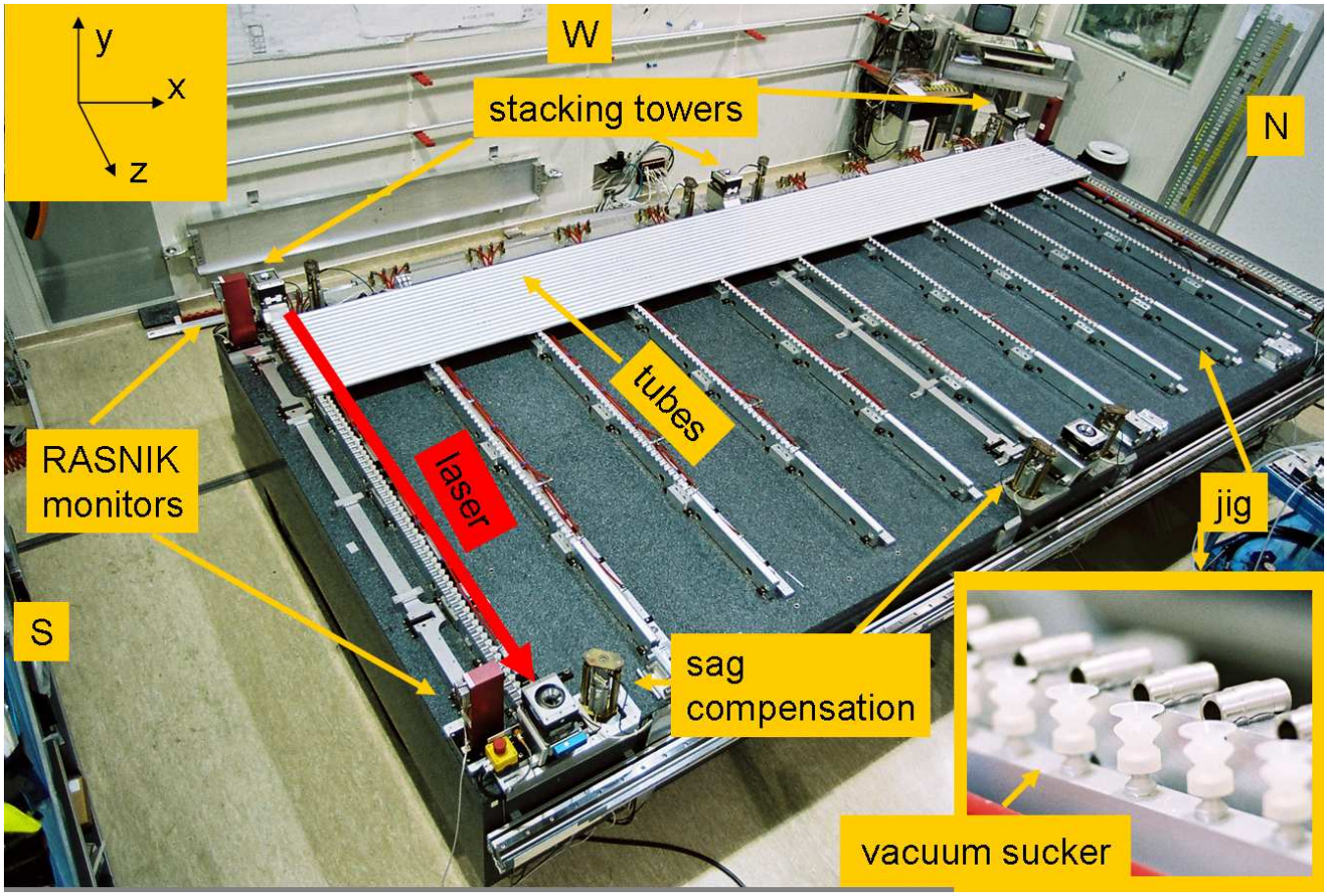

Figure 15: *Picture taken in the cleanroom showing the assembly table. Several key items are indicated.*

the spheres with so-called sphere-holders that can move freely in the x direction to absorb temperature variations. For this same reason, at the east side (the non-reference side), the sphere-holders can move freely in the horizontal plane. The sphere-holders are designed such that their height during possible horizontal movements is maintained with an accuracy better than a few microns.

When the spacer (with or without already fixed tube layers) is supported by the stacking towers the gravitational sag of the cross plates is considerably, of the order of 50 μm . To reduce this sag to typically 10 ± 10 μm , the unfinished chamber is carried by an additional system utilizing pneumatic supports. One of the eight pneumatic cylinders constituting this system is also visible in figure 16b.

After the construction of every 25-th chamber several checks concerning the accurate positioning of the mechanics are performed. Notably, the distances between the corner stacking towers and the corresponding jig at the RO and HV reference side is measured with an auxiliary device. When these distance deviate, the chamber obtains an unwanted stereo angle build in. Our checks demonstrated that such stereo angle is smaller than 4 μrad over the full period of the production.

3.2 Chamber assembly

The assembly procedure starts outside the cleanroom with the construction of the bare spacer, with a 'loose' accuracy of typically 500 μm . Then, in the cleanroom, the tubes are attached layer by layer using glue. This process typically takes half a working day, but the time needed for the glue to cure, constraints the production-speed to one layer a day.

As already mentioned the quality control during chamber assembly start with re-measuring the wire tension

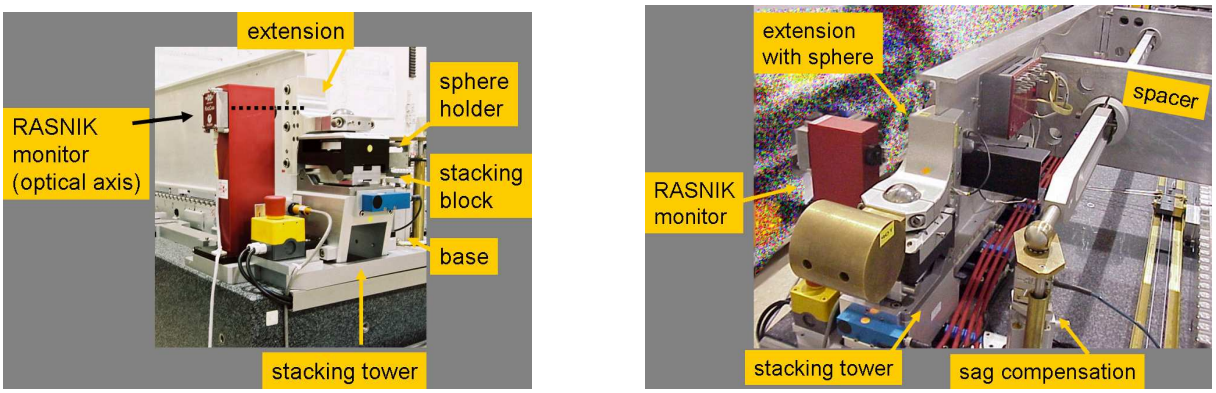

Figure 16: *a) The picture shows the stacking tower supporting the sphere in the extension of the spacer. The position of the extension is monitored by a RASNIK alignment system. b) This pictures shows the stacking tower together with the sag compensation tower.*

of the tubes to be glued in the particular sequence. After this test, the tubes are positioned in the jigs and the gas jumpers are temporary fixed in a way such that tube length differences within a triplet are absorbed as illustrated in in figure 17, which ensures a tight connection of the jumpers on the tube. Additionally, to position the end-caps of an entire tube layer in-line, we use jumpers of appropriate thickness (in steps of 100 μm , maximal 300 μm), which later on facilitates the the mounting of electronic boards.

After this procedure, the jumpers are loosened to avoid unwanted stress between neighboring tubes that could prevent the tubes to fall into their jig position. Then, the position of the end-plugs, both at the RO and HV side, is measured using a laser beam running parallel to the end-plugs [5] as indicated in figure 15. For this test, a reference rod is placed between two adjacent tubes which partially blocks the laser beam measured by an optical sensor. Deviations in the response represent a measure of deviations in tube heigts. Note that by measuring between adjacent tubes, the results of this test are somewhat ambiguous in case neighbouring tubes are both badly poistioned. In addition, the test is sensitive to tube heights (y) as well as to the distance (z) between tube pairs and the radii of the corresponding end-plugs. On the other hand, a badly positioned tube shows up twice and is tagged easily. In practice, only a few tubes needed to get re-positioned. In some rare cases, we had to replace the complete tube due to, as it turned out, bad swaging of the end-plug. Bad swaging occurred for a particular batch of tubes where the end-plug was not well inserted in the aluminium tube. We aimed at tube height deviations below 20 μm and all tube pairs above 10 μm were inspected by the operators. The result of these measurements as shown in figure 18, indicate that the tubes are well positioned.

After position of the tubes glue is dispensed by means of an automated gluing machine as shown in picture 19a.

For the first (and later second layer), glue (Araldite 2019) is dispensed only in between adjacent tubes. The relevant side of the cross-plates is supplied with a sufficient amount of glue (DP490, 3M) and the spacer is lowered onto the tube layer. The correct positioning of the spacer is checked using the RASNIK systems

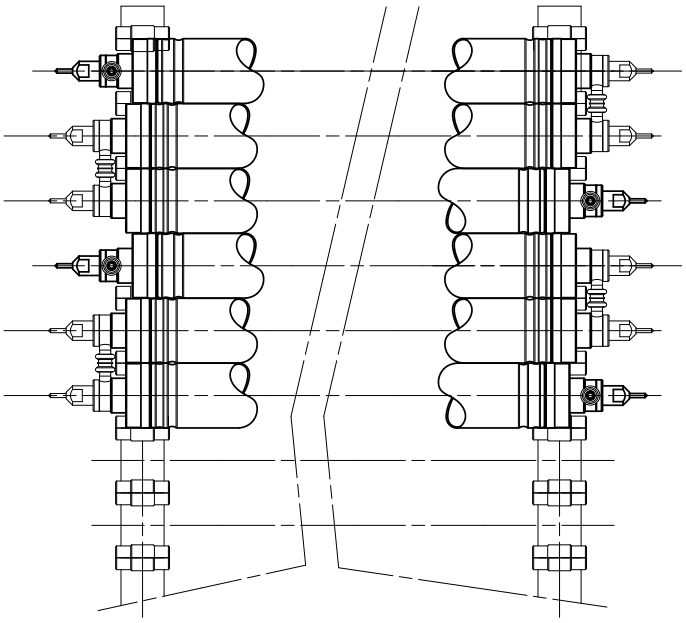

Figure 17: *Illustration of the tube positioning in the jigs prior to gluing. The tubes are connected in triplets that connect to the gas manifolds. The gas jumpers are firmly fixed, aligning adjacent tubes of the same triplet.*

that monitor the cross-plate extensions at the four stacking towers at the corners of the assembly table. In addition, we used a temporary RASNIK system on both the HV and RO crossplate to monitor their sag. These RASNIK systems provided crucial position information with high precision that allowed to solve all occasional problems prior and during gluing of tube layers.

After glue curing for at least 12 hours the spacer with the first tube layer is rotated upside down, effectively over its z axis, thus respecting the reference side. The second tube layer is prepared the similar procedure as for the first layer is followed. Now both sides of the spacer have a tube layer attached to it. To glue the third layer, the spacer is lifted and the stacking tower height is adapted to attach the third tube layer. On the tubes of the third layer and onward, two additional glue ropes (Araldite 2011) are dispensed to connect adjacent tube layers. To glue the fourth layer, the spacer with its three tube layers is rotated back to its original orientation, limiting the (un)balance of the spacer and tube layers and thus avoids possible effects of asymmetrical weight distribution. After gluing the fifth layer, one multilayer with three tube layers is finished. Figure 20 shows the distribution of glues between the tubes in a finished multilayer. The chamber is turned once more to finish it by attaching the sixth layer. A picture of the final chamber still on the granite table was already shown in figurebolaf.

3.3 Automated assembly manager

To routenily produce the muon chamber an automated assembly manager has been develloped. It steers the actions of of the operators and provides detailed information of the corresponding assembly step using

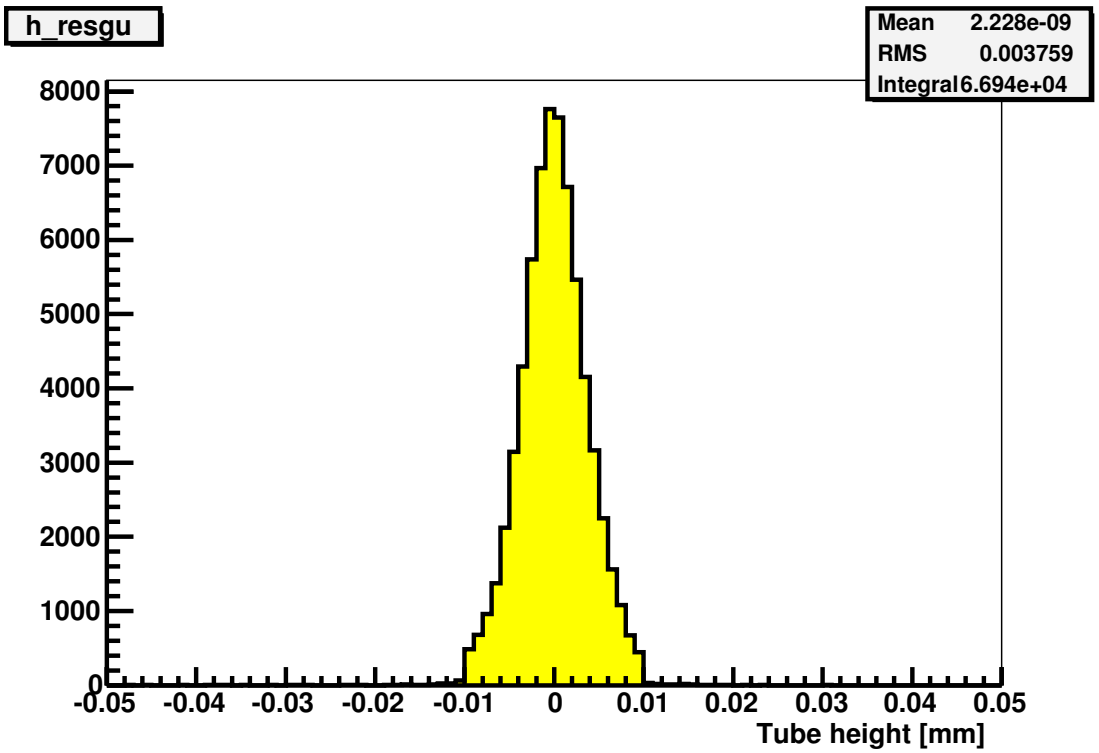

Figure 18: *Tube positions during assembly.*

a web-interface. Moreover, this manager monitors and logs relevant parameters and issues warnings when neccessary.

Figure 19: *a) Glue dispension by the gluing machine. b) attaching another layer.*

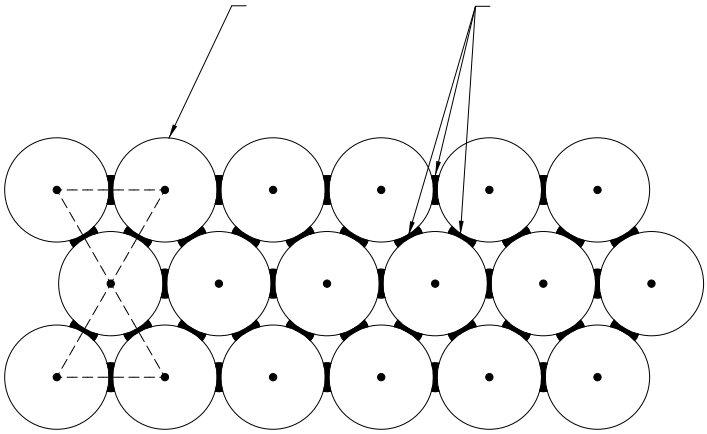

Figure 20: *Illustration of the distribution of glue between the tubes in a multilayer.*

4 Chamber services

After mechanical assembly, the chamber leaves cleanroom to mount additional gas, control and read-out services. These on-chamber services are designed for stable long term operation, but with the possiblity to replace the main components. This resulted into a design with a limited number of connections to the 'outside world', allowing relatively easy chamber testing and installation. This section summarizes the services.

Alignment components As mentioned before, physical deformations of the chambers are monitored with the in-plane alignment system consisting of four RASNIK systems mounted during chamber construction. This system is calibrated just after glue curing of the final tube layer when the chamber is still on the granite table. The components for the in-plane RASNIK systems are shown in figure 21. The power and readout for all alignments systems is provided by an on-chamber multiplexer, called RASMUX, which itself is later connected through one D-25 cable to a master system that steers and collects information of several muon chambers.

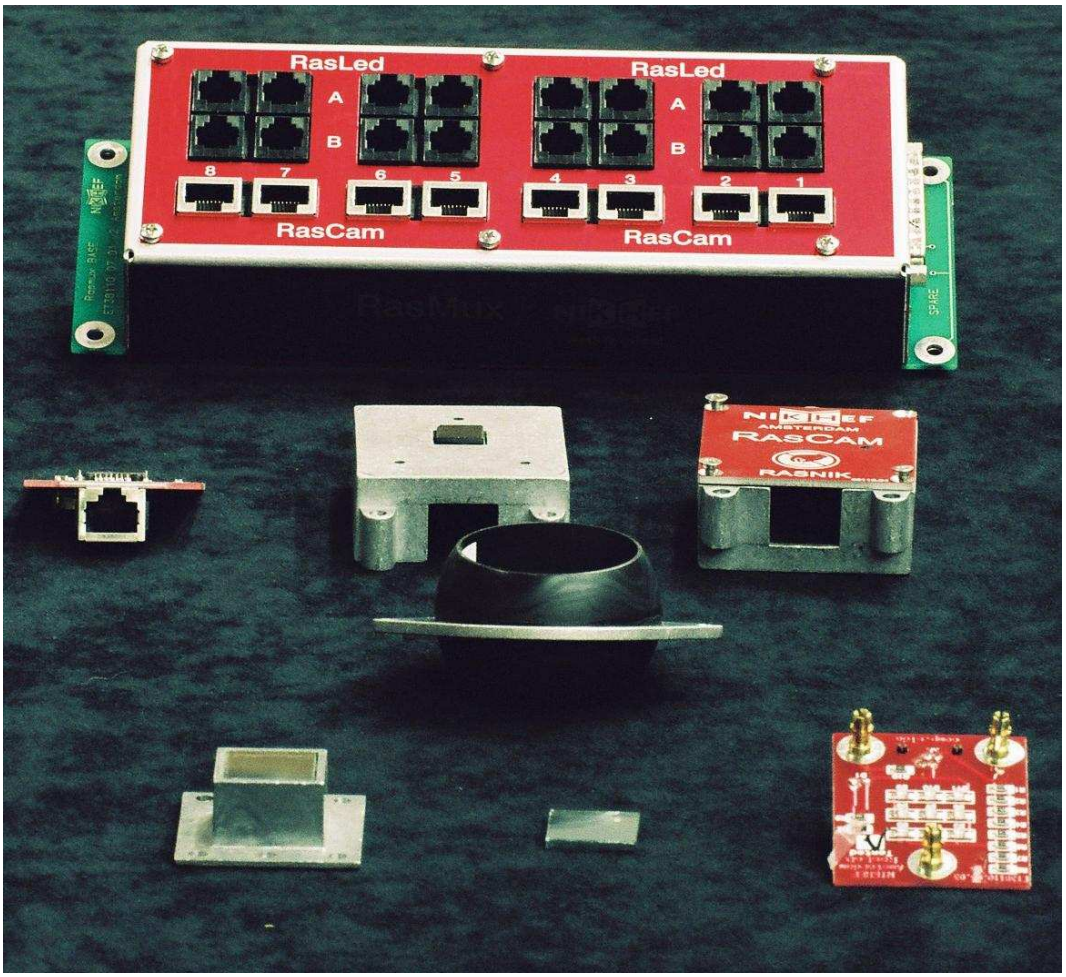

Figure 21: *Picture of several alignment components.*

The inter-chamber alignment consist of RASNIK systems monitoring the position of neighbouring chambers of the same type and RASNIK systems that monitor the projective alignment of the three muon

chamber layers. In a test setup at CERN [6] it was demonstrated that this system, after calibration with cosmic ray tracks, achieves an alignment accuracy better than 10 μm (on the change of the relative chamber positions). After chamber construction the mounting platforms for these systems are positioned and glued on the chambers with an estimated accuracy of 100 μm . The corresponding RASNIK components are calibrated to higher accuracy on a special test bench to provide absolute alignment calibration just after installation in ATLAS. This calibration, limited by the accuracy of the platform positions, will then be superseeded by the alignment with tracks in the commisioning phase of the experiment.

Temperature and magnetic field sensors A total of 18 temperature sensors provide supplementary information on possible chamber deformations. In addition, typical a few magnetic field sensors probe the field for off-line corrections. These sensors connect to the detector control system (DCS). The DCS is configured and readout with the CAN protocol.

Gas system The on-chamber gas system consists of two gas manifolds for each multilayer. In figure 22

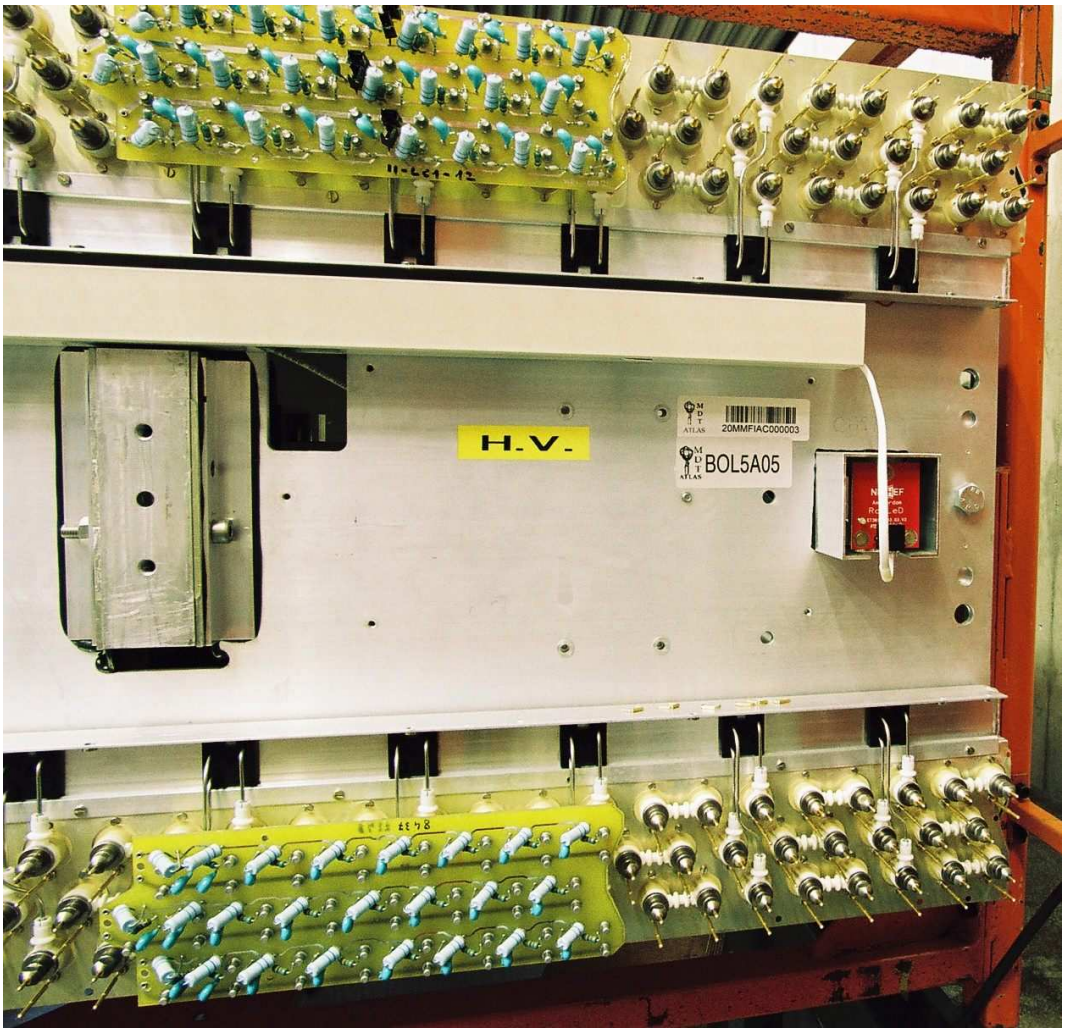

Figure 22: *Picture taken the HV side of a BOL chamber. Some individual tubes can be recognized together with the connections to the gasmanifolds. Also shown is a HV board and the backplate of the RASNIK mask component.*

can be seen that tubes of the same layer are grouped in series of three (tripplets). Only the first and last tube in the tripplet connects to the manifold at the RO side and HV side respectively. After installing the

gas system, the chamber is filled to 3 bar and its pressure (corrected for temperature effects) is monitored for at least 24 hours to assure the gas tightness of the added components. The manifolds have only one input or output and can be quickly connected to the gas service in the experiment.

Electronics As can be seen in figure 22, the RO and HV electronic boards are connected to signal and the ground pins of groups of 24 tubes. The RO and HV electronic boards are therefore provided with xxxxxxxxxxconnetors to connect to the pins robustly.

The electrical lines on the HV boards are interconnected layer by layer and connect to the on chamber HV disribution box.

At the RO side, the boards amplify the analogue electrical signals..... The digital signal processing and the final time measurement is performed by the so called 'mezzanine' cards that directly connect to the analogue RO electronics and are housed in individual faraday cages. The digitized signals are shipped to a central on chamber processor card (CSM) as shown in figure 23. The CSM is configured via the DCS and connects to the data acquisistion system by optical fibers.

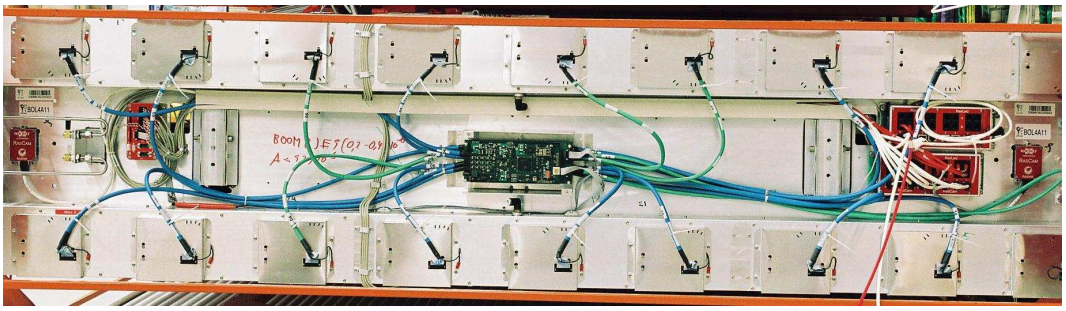

Figure 23: *Picture taken at the RO side of a nearly completed BOL chamber. The RO electronics of the top and bottom multilayer is enclosed in Faraday cages. Also visible are the backplates of the RASNIK cameras, the DCS control box for the temperature and B field sensors, the readout motherboard and two RASMUXes as required for this specific chamber.*

5 Tests of completed chambers

Have we produced chambers with mechanical accuracy below 20 μm ? How do the chambers behave under large temperature variations? Do the chambers operate stable under nominal pressure and HV conditions and can we measure muons? Several tests are performed to adress these questions. The most important results are summarized in this section. We refer to the chambers as BOLx, where 'x' is the production number of the chamber. A special case is BOL0, which is the so-called module-zero chamber. This chamber was assembled and tested prior to the assembly of the 100 production chambers to demonstrate that we can fullfill the requirements.

5.1 Results of X-ray scans

About 10% of all chambers undergo a mechnical precision check in X-ray tomograph [7] at CERN. The tomograph consists of a unit with two stereo X-ray beams that runs over the chamber in the z direction

at a fixed x position. Scintillator counters measure the 'shadow-pattern' of the wires and tube-walls. A dedicated analysis of such pattern results in a wire position map with an accuracy of typically 5 μm . The chamber is considered certified as the distribution of the residuals with respect to the nominal wire map has an RMS below 20 μm .

5.1.1 The nominal wire map

The nominal wire map is obtained from the scan of the BOL0 chamber and is parametrized by five parameters as listed in table 1.

Parameter	Nominal value
Stereo angle between multilayers ($d\alpha$)	0 μrad
Shift in the horizontal direction between multilayers (dz)	0 μm
The y distance between the multilayers (y_{dist})	346.924 μm
The z-pitch-30mm of the tube layers (Δz_{pitch})	35.40 μm
The y-pitch of two adjacent tube layers in the same multilayer (y_{pitch})	26.027 mm

Table 1: *The table lists the parameters that determine the nominal wire map.*

Since we know all the dimensions of the precision mechanics on the granite assembly table, a prediction of the nominal wire map could be made. This turns out to be far form straigthforward and large corrections caused by glue shrinkage have to be understood as is described in Appendix B.

Anyway, the key issue is whether BOL0 and all following production chambers are represented by the nominal wire map. For BOL0, the tomograph scan yielded an RMS of 16 μm for the residual distribution of its wire positions with respect to the nominal wire map, well below our stringent requirements. An overview of the results for all scanned chambers is presented below.

5.1.2 Mechanical accuracy of BOL chambers

The chamber is scanned in the tomograph and the actual wire positions are reconstructed at at least four positions along the tubes. Usually, about 15% of the wires is not recontrcted due to the shadowing of the X-rays by the longbeams. Close to RO and HV cross-plates, where the wire is fixed, the position is determined by the end-plugs, while more centrally the accuracy of the wire tensions plays a compatible role. We decided to list the accuracy of the wire positions at either RO or HV cross-plate. Usually the results at both sides are very similar; we list the worst RMS value of the two, also separate for the z and y projection, in table 2. Also given is the percentage of wires that was reconstructed from the X-ray tomogrgaph measurements. It appears that all but one chambers easily fullfill the precision requirement of 20 μm RMS. In fact, most chamber are well below our requirements. Note that all results are obtained using the nominal wire map as discussed above. The worse result for BOL94 is a bit surprising and is..... xxxxxxxxxxxxxxxx.

5.2 Broken wires

xxxxxxxxxxxx. After the completion of the first chambers we detected a number of broken wires in several chambers Most wires snapped in the wire locator of the end-plug, but several broke around 40 cm away from the end-plug. Despite many dedicated studies, the cause of this problem has not been recovered. However, we observed that broken wires seem to occur only in chambers that have 'seen' high gas flows ($>$ 1 bar l/s). Moreover, this problem is restricted to the first (or last) tube of a triplet connecting to the gas manifold. To avoid such high flows we put mechnical flow restrictors in the on chamber gas outlet tubing. In total we have xxxx chambers with broken wires. Usually, the number of broken wires is limited to one

Chamber	RMS z (μm)	RMS y (μm)	RMS combined (μm)	% of wires reconstructed
BOL0	16.7	12.7	14.8	74%
BOL2	12.9	18.7	16.1	67%
BOL3	16.1	14.0	15.1	81%
BOL7	13.2	13.1	13.2	85%
BOL7	10.7	14.3	12.6	93%
BOL8	12.8	15.7	14.3	86%
BOL9	12.8	15.4	14.2	88%
BOL11	16.1	16.4	16.2	87%
BOL11	15.8	17.0	16.5	83%
BOL48	12.4	14.4	13.4	94%
BOL50	10.5	15.0	13.0	79%
BOL59	15.3	20.6	18.2	90%
BOL61	13.1	19.6	16.6	86%
BOL65	16.2	17.1	16.7	81%
BOL71	14.9	20.2	17.8	77%
BOL90	7.5	16.3	12.7	84%
BOL94	24.1	26.9	25.6	86%

Table 2: *The table lists the residuals of the wire coordinates obtained in the X-ray tomograph. The number of the BOL chamber refers to its serial production number. The percentage of reconstructed wires is also given.*

or two, except for one chamber, which has 11 broken wires. We repair the broken wires, using a procedure that uses the existing o-ring and thus not requires any glue. This comes not for free. The accuracy of the wire position is estimated to a few 100 μm . In principle, the wire position of such wires can be obtained later in the ATLAS experiment with a procedure that uses tracks.

Our main worry now is whether the breaking of wires is a continuing process. "Bob Dylan, once song: How many wires have to snap before we call it at end? The answer, my friend, is blowing in the wind xxxxxxxxxx." After storage, handling and transporting, the chamber are now being installed in the ATLAS experiment. Just before installation a final check procedure has revealed no evidence of newly broken wires xxxxxxxxxx.

5.3 Cosmic ray test facility

The main purpose of the test facility is to verify the electronic read-out and performance of each chamber under ATLAS conditions (Ar/CO_2= 93%/7% at 3 bar and HV = 3100 V) conditions.

The cosmic ray test facility at NIKHEF accomodates five BOL chambers and has a fixed trigger system as shown in figure 24. The trigger units (also visible in the figure) consist of two layers of scintillators, separated by 50cm thick iron block to reject low energetic muons (i.e. muon with energies below 0.7 GeV). Since the summer of 2004 till the autum of 2005 routinely BOL chambers have been tested; usually the three chamber middle chambers were exchanged and the outer chambers were kept in place as a stable reference.

5.4 Results

An analyis of the data taken with the cosmic ray test facility was performed in steps and several distributions were studied. The first step consist of a determination of the minimal and maximal drift time, t_0 and t_{max} respectively, from the measured drift time spectrum.

Figure 24: *Picture of the NIKHEF cosmic ray test facility with five BOL chambers. The chamber in the in the highest position is - in this particular case - a small type BOL chamber with a width of 48 tubes, the others are standard BOL chambers.*

The t_0 and t_{max} values for each individual wire were determined by fitting a threshold function to the drift time spectrum. In Figure 25 the t_0 and t_{max} values for BOL002 are shown. Large deviations from the nominal values are a good indicator for problems. In some datasets a pattern related to groups of three drift tubes constituting a gas-tripplet was observed. After an extended period of flushing this pattern disappeared. One problem remained: the broken wires observed in some chambers as mentioned above. A broken wire - if present - is spotted by searching for a hole in the hit distribution. A typical hit distribution for BOL002 is shown in Figure 26. After a broken wire was been found, the wire was replaced.

In a second step, the drift distance versus time or r-t relation is determined using the so-called autocalibration method. An initial guess of the r-t relation is used from previous calibrations. Using this relation, a full pattern search and track fit is performed and the residuals of the hits w.r.t. the track fit are determined. These residuals as a function of the drift time are then apllied as a correction to the initial r-t relation. This process is repeated till convergence has been reached. Using the calibrated data, the average resolution per tube is determined as shown in Figure 27. The average resolution is about 70 μm.

By selecting well-reconstructed tracks and checking whether a track crosses the sensitive volume of the tube, the hit efficiency per tube is determined from the data. The distribution for BOL002 is shown in Figure 28. The hit effiicciency is well above 99.7%.

Also other distributions were studied to look for possible problems. Large wire displacements could be observed by constructing an observable using the residuals. In Figure 29 the wire position in the precision plane is shown for BOL002. The results are compatible with no shift within an error of 100 μm.

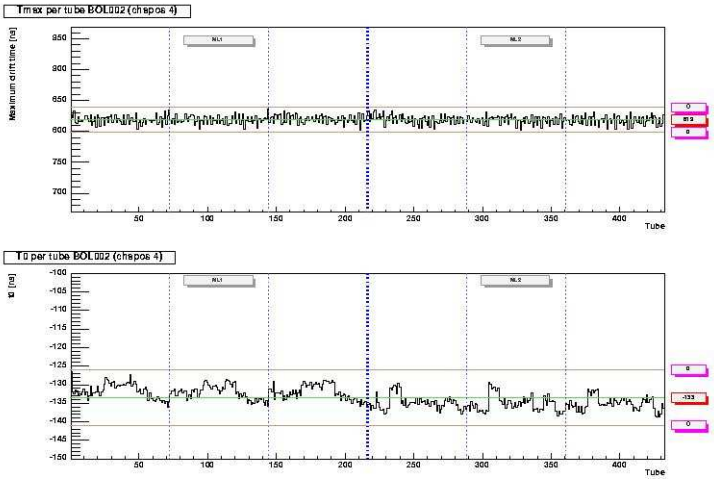

Figure 25: *The t_0 and t_{max} distributions for BOL002 as a function of the tube number.*

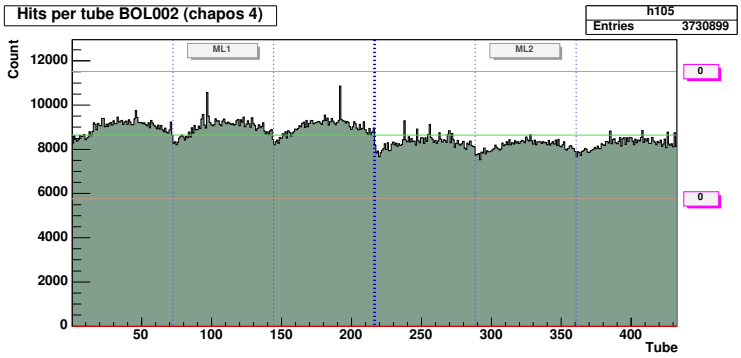

Figure 26: *Hit distribution for BOL002 as a function of the tube number.*

5.5 Effects of temperature gradients

In some places in the ATLAS experiment, the temperature of the air surrounding the BOL chambers is expected to reach gradients as large as 5 degrees. Estimations vary, but over a chamber, between the multilayers, we should be prepared for gradients of 1 degree.

The chambers are constructed from aluminium that expands typically 24 μm /m/K. Overall temperature changes are not seen by the inplane alignment system, but are monitored by the temperature sensors and can relatively easy be corrected for. In contrast, chamber deformations due to temperature gradients are more difficult to monitor and to correct for. The two 'first order' effects are the sag of the whole chamber (comparable with a graviational sag) and the sag of the cross-plates. This implies that the chamber should not sag more that 100 μm /K to keep the wire sufficiently centered and the cross-plate should not sag more than 20 μm /K to avoid large effects (and off-line corrections) on wire postions.

We conduct a small experiment by covering the BOL0 chamber (in its horizontal position) by electrical heat blankets. These blankets produce 50W/m^2, leading to gradients of several degrees over the multilayer (away from the cross-plates). The sag of the chamber and cross-plates are measured by the in-plane alignment system and additional RASNIK systems along the cross-plates. It takes approximately three hours for the temperatures to reach stable values for which the results are listed in table 3. For the chamber and cross-plate sag we obtain 50 μm /K and 6 μm /K which is below our requirements.

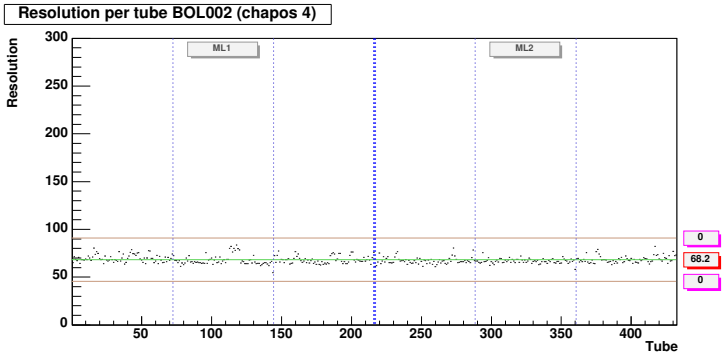

Figure 27: *Resolution for BOL002 as a function of the tube number.*

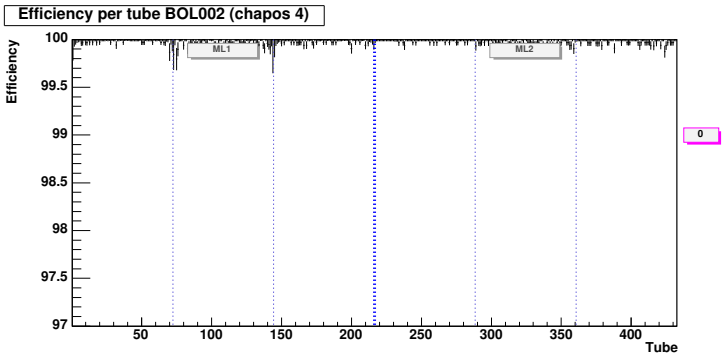

Figure 28: *Efficiency for BOL002 as a function of the tube number.*

6 Conclusions

xxxxxxxxxxxxxxxxxx At Nikhef in Amsterdam we have produced 100 large muon chamers (inclusing 4 spares) for the ATLAS experiment at the LHC (CERN, Geneva). The 5m long and 2m wide chambers consist of several layers of aluminium drift tubes, which are glued together under well controlled conditions. xxxxxxxxxx

Some chamber were operated using high gas flows and have broken wires. Several studies have not revealed the cause of this problem, but there appears to be a correlation with high gas flow through the drift tubes. We have found no evidence, even not after transporting the chamber from Amsterdam to Geneva, for spontaneous wire breaking. xxxxxxxxxx

The aimed mechanical accuracy on the wire positions is well below 20 μm RMS. Tests of the chambers operating at nominal HV and pressure in a dedicated cosmic ray set-up show stable results. xxxxxxxxxxxxxxxxx

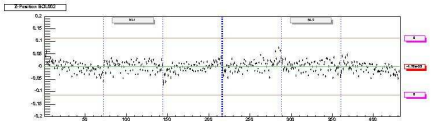

Figure 29: *Wire position deviation in the precision plane for BOL002 as a function of the tube number.*

Quantity	Effect	Effect Normalised to 1K over ML
T gradient over multilayers	4K	1K
T gradient over cross-plate	$\approx$0.3K	0.1K
T gradient over tube-layers in ML	$\approx$0K	0K
Chamber Sag	200 μm	50 μm
Cross-Plate Sag	25 μm	6 μm

Table 3: *The effects of heating the BOL0 chamber using electrical blankets.*

References

[1] The ATLAS MUON TDR, http://atlasinfo.cern.ch/Atlas/GROUPS/MUON/TDR/Web/TDR.html

[2] The Pavia-Roma1 ATLAS MDT Quality Control System. C. Bini et al. 2001. Nucl.Instrum.Meth.A461:65-67,2001

[3] An electromagnetic micrometer to measure wire location inside an ATLAS MDT drift tube, Cambiaghi, M., Cardini, A., Ferrari, R., Gaudio, G., ATLAS Internal Note ATL-MUON-1998-259, 1998

[4] Electrostatic digital method of wire tension measurement for KLOE drift chamber. A. Andryakov et al.. 1998. Published in Nucl.Instrum.Meth.A409:63-64,1998

MDT wire tension measurement using an electrostatic method, ATLAS internal note, ATL-MUON-38-264.

[5] A QA/QC system to monitor the planarity of the tube layers in MDT chambers construction G. Ciapetti, G. De Zorzi, R. Giacalone, L. Montani, D. Pinci. ATLAS Internal Note MUON-NO-29 September 1998

[6] First System Performance Experience with the ATLAS High Precision Muon Drift Tube Chambers Poster presented by M. Vreeswijk at Vienna WCC 1998. Published in Nucl.Instrum.Meth.A419:336-341,1998
http:atlasinfo.cern.chAtlasGROUPSMUONdatchadatcha.html

[7] High precision X-ray tomograph for quality control of the ATLAS muon monitored drift chambers. J. Berbiers et al. 1998. Published in Nucl.Instrum.Meth.A419:342-350,1998

A Alignment system RASNIK

The Red Alignment System NIKhef (RASNIK) consists of a coded mask, a lens and a video image sensor. The mask, illuminated with (infra-red) LEDs from behind, is projected by the lens onto the image sensor as illustrated in figure 30. A daylight-blocking filter is placed before the image sensor. If the lens is displaced

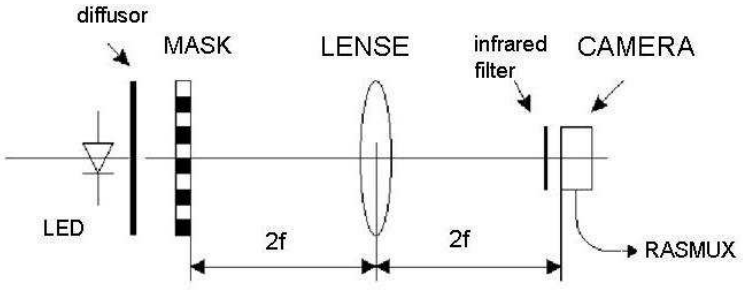

Figure 30: *The principle of RASNIK.*

in the direction perpendicular to the optical axis, then the image on the sensor will be displaced in the same direction, magnified with a factor $(v + b)/v$, where v is the object distance and b the image distance. If the lens is displaced along the axis, the image scale S will change following $S = b/v$. Finally, if the mask rotates around the optical axis with respect to the sensor, the image rotates accordingly. From the analysis of a RASNIK image, four parameters can be deduced: two tranversal displacements, one displacement

along the optical axis, and the relative rotation between the mask and sensor around the optical axis. The changes are relative: a common shift of three components does not change the readout values. The changes can be expressed, for instance, in terms of a mask displacent or a lens displacement.

A typical RASNIK image is shown in figure 31, clearly displaying the chessboard pattern, in which each 9th row and 9th column is carrying a digital code. This code has the values (0,0) in the bottom left of the masks, and increases linearely with the coded column and row numbers into the direction of the top-right corner in the mask. In this way the coarse position of the image, showing only a small part of a large mask, can be identified.

The video signal of the sensor is digitised by means of a frame grabber in a pc. After differentiating the image data, the contours of the chess fields appear as an orthonormal grid pattern. From this, the 'fine' image position, image scale and image rotation are obtained. After detecting and decoding the 9th row and columns, the coarse image position is obtained.

Due to the large summed length of chess field contour on an image (100 mm, in both directions), a precision of 50 nm (RMS) is obtained in the two transversal directions in terms of image position on the sensor, per image. The image scale is measured with a resolution better than 5×10^{-5} (RMS), and the resolution of the image rotation is 20 μrad (RMS). When placed in air, the RASNIK performance is limited by the gradients and fluctuations in the gradient of the air temperature. The linearity of the system is exclusively determined by the precision of the mask. For ATLAS, we applied low- cost 'contact copies' of mother-masks made in VRSI industry, and their precision was guarantied to be better than 0.1 μm . The range of a RASNIK system is determined only by the mask size, and can be as large as 125 $\times$ 125 mm^2. For the InPlane systems we applied mask segments of 20 $\times$ 20 mm^2, and for the projective systems masks of 50 $\times$ 50 mm^2 were used.

A RASNIK system can be calibrated by placing the three components in a well known relative position, while recording the readout values. After that, the deviation from the initial alignment can be obtained from the difference between the actual readout values and the calibration values.

B Prediction of the nominal wire map

The nominal wire map for BOL chamber is determined in X-ray scan of the BOL0 chamber, see Table 1 in section 5.1.1. For this section, the most relevant results are:

- The y distance between the multilayers (y_{dist}) 346.924 μm ,
- The y-pitch of two adjacent tube layers in the same multilayer (y_{pitch}) 26.027 mm,

An interesting study is the following. Since we know all the dimensions of the precision mechanics on the granite assembly table, a prediction of the nominal wire map can also be made. A naive approach leads to $y_{dist} = 347.010\ mm$ and $y_{pitch} = 26.011\ mm$, indicating that the space between multilayers (see table 1 again) has shrunk by 86 μm , while adjacent tube layers are less closely packed (by 16 μm). This observation can to a great extent explained by:

1 The two inner tube layers that attach directly to the cross-plates are positioned closer to the crossplate than foreseen. During gluing, the sag of the (outer) cross-plates is only partially compensated by the pneumatic system as mentioned above to the level of 15 μm as can be seen in figure 32. The effect is not constant along the cross-plate; it has a parabolic shape which has a maximum size near the centre of the cross-plates.

  The shrink of the glue during curing which amounts to 1% of its thickness and thus increases the effect by another 5 μm has an additional effect on the sag of 10 μm , also visible in figure 32.

If we add these numbers we find 30 μm with an uncertainty of at least 10 μm and a decrease of the distance between the two inner layers of 60 μm . This is close to the 84 μm which is observed in the tomograph.

2 Another effect that affects the middle tube layers in both multilayers and the outer tube layers is also related to the sag of the cross-plates. The nominal space between adjacent tube layers is only 26 μm at the end-plug. The glue used here is relatively a-viscous and when hte spacer is lowered on the ready to be glued new layer it is somehow partially carried by the glue and thus not entirely by the precision towers. Figure 32 supports this explanation. Obviously, this affect the distance between tube layers and also shape of the sag. We searched for more evidence of this effect and we used the data from BOL0 to BOL8 for a dedicated. The distance between adjacent tube layers is extracted from the rasnik system and the results are shown in figure 33. Remarkably is that the effect for the middle tube layers increases during glue curing. Anyway, the increase of the pitch is on avarage 15 μm , in agreement with the 16 μm measured by the tomograph.

From the above we conclude that the rasnik results are consistent with the the measurement of the tomograph. Finally we want to remark that most effect discussed in this section increase (quadratically) with the witdh of the chamber under construction. Since the BOL chambers are among the largest ATLAS muon chambers the result is satisfactory.

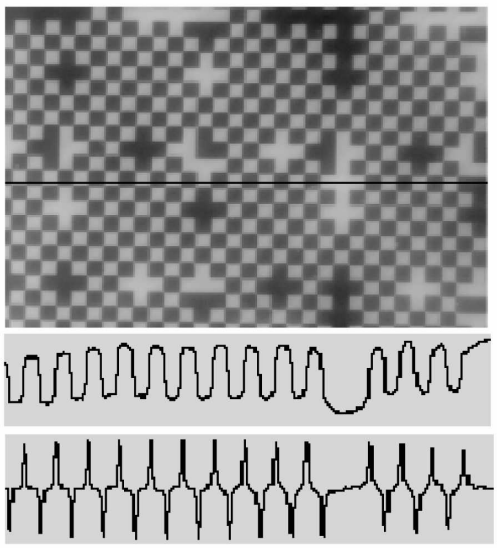

Figure 31: *Typical RASNIK image with the chess sboard pattern and the coded row and columns. The light intensity of the pixels under the indicated line is plotted, together with its derivative. The Gaussian peaks (positive and negative) determine the fine position of the image, as well as the image scale.*

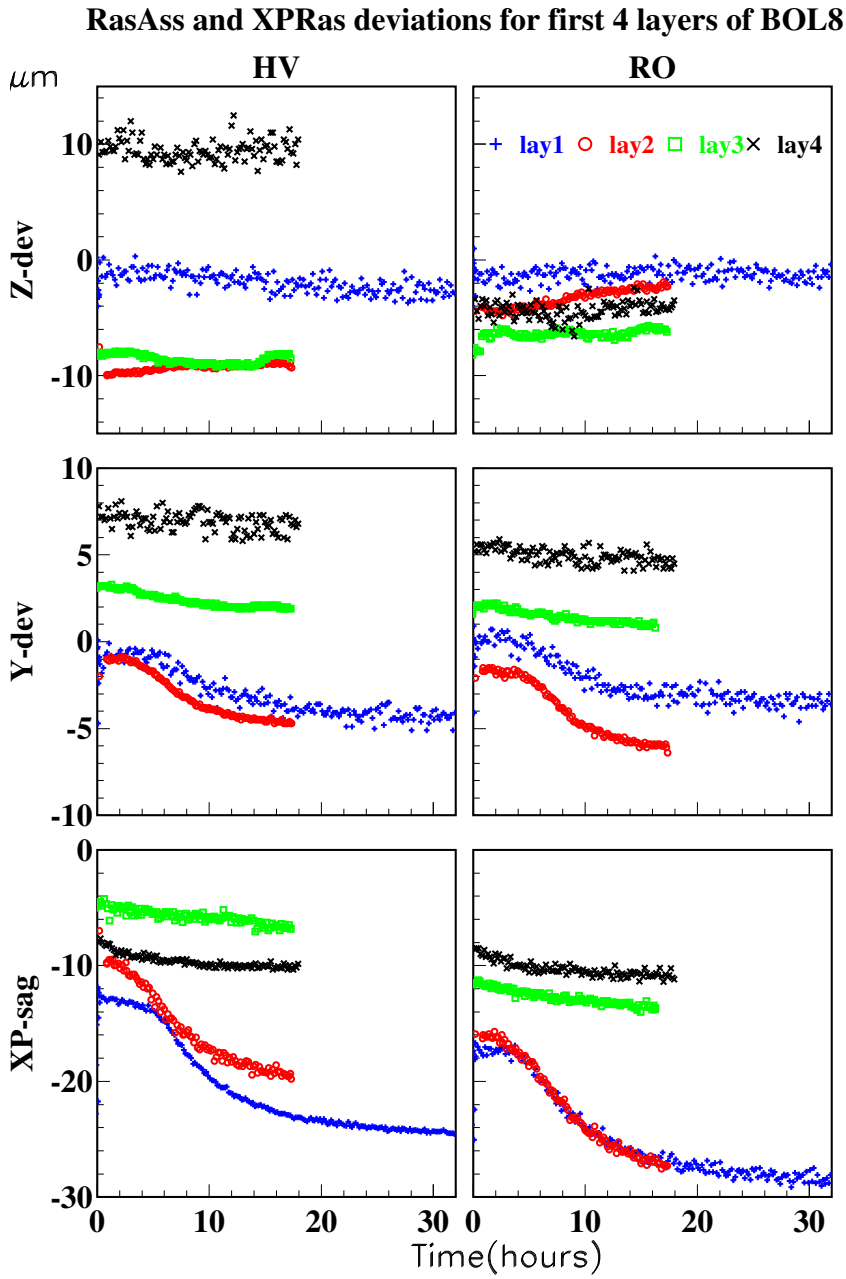

Figure 32: *Rasnik data for BOL8 as function of time since start of glueing for layers 1 to 4. The upper plots show the z values from the reference side at the HV and RO side of the chamber. The middle plots show the average of the y values at the reference and non-reference side. The lower two plots display the cross-plate sag seen by the cross-plate rasniks. The systematic change in Y and cross-plate sag for layers 1 and 2 is attributed to glue shrinkage as explained in the text.*

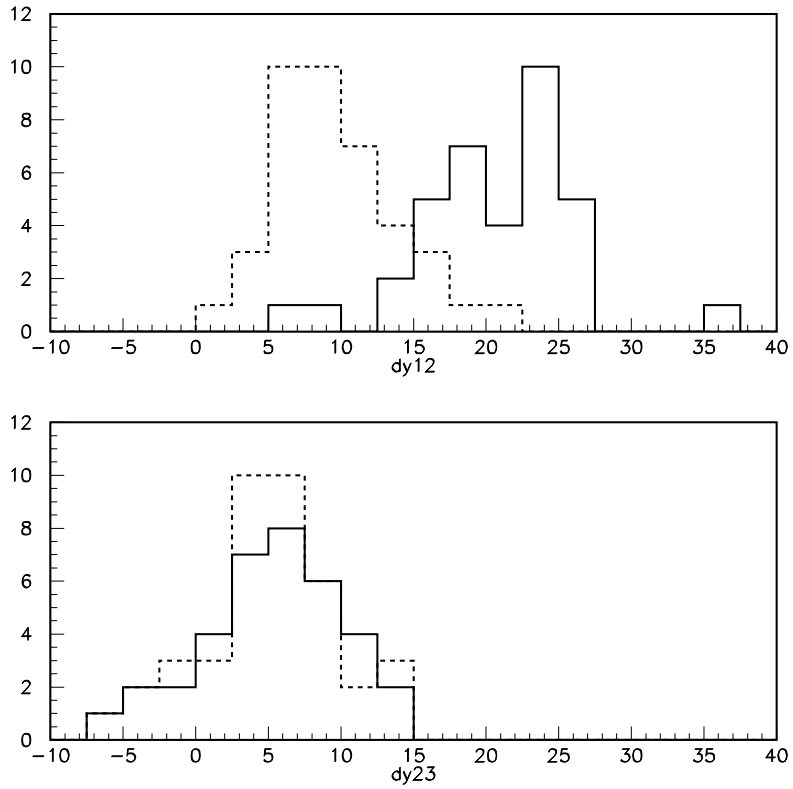

Figure 33: *The deviations from the nominal Y pitch between layers for chambers BOL0 to BOL8 as derived from the rasnik systems during glueing. The upper plot shows the deviations for the inner two layers within a multilayer (dy12) and the lower plot for the outer two layers (dy23). The data are plotted at the start of glueing (dashed line) and after the glue has cured (solid line).*